Zahn, R., Comas, M.C., and Klaus, A. (Eds.), 1999
Proceedings of the Ocean Drilling Program, Scientific Results, Vol. 161

20. THE HIGH-GRADE BASEMENT OF THE ALBORAN SEA: STRUCTURAL AND PT EVOLUTION[1]

Giacomo Prosser,[2] Piera Spadea,[3] and Carlo Doglioni[2]

ABSTRACT

The Alboran basement recovered at Site 976 is characterized by a low-pressure (P) and -temperature (T) metamorphic overprint and resembles the higher Alpujárride nappes of the Betic Cordilleras. The basement, consisting mainly of Al-rich metapelites with interlayered marbles and calc-silicate rocks, records a polyphased deformation and metamorphic history. A metamorphic evolution characterized by decompression and heating can be recognized between the first (D_1) and second (D_2) deformation events. This evolution is documented by a decrease of spessartine and grossular toward the rim of garnet growing between D_1 and D_2, and the lack of staurolite during and after D_2. The presence of cordierite and hercynite in the T-peak assemblage is an additional evidence of a T increase associated with a significant drop in P. Partial melting is locally revealed by cordierite-bearing leucosomes, which cut across the S_2 schistosity of the high-grade gneisses. The PT conditions attained during peak metamorphism were estimated by conventional thermobarometry to be ~700°C and 2.8–4.4 kbar. The peak metamorphic conditions were followed by the growth of andalusite porphyroblasts and by sillimanite-bearing mylonitic bands (D_3). Contemporaneous heating and decompression is consistent with crustal thinning coupled with magmatic underplating during the exhumation of the Alboran basement. The thermal anomaly induced by this geodynamic process decayed rapidly, as seen in cataclastic bands that directly cut the high-T rocks, with rare low-T plastic deformation.

INTRODUCTION AND GEOLOGIC SETTING

Unraveling the structural and pressure (P) and temperature (T) evolution of high-grade basement rocks is sometimes a difficult task. During high-temperature metamorphism, intense ductile deformation easily erases traces of previous foliations, and high-T annealing overprints textures and fabrics developed in localized high-strain zones (Passchier et al., 1990). Moreover, microstructural evidence indicating the timing of mineral growth often yields conflicting conclusions (Vernon, 1996). In the high-grade rocks of the Alboran sea, these problems can be solved because older foliation-forming events are recorded as inclusion trails in minerals (especially garnet [Grt]), and sillimanite (Sil) -bearing shear-zones can be recognized in spite of later high-T annealing.

The basement rocks recovered by Ocean Drilling Program (ODP) Leg 161 are composed of medium- to high-grade schists and gneisses, with associated migmatitic gneisses, marbles, calc-silicate rocks, and leucogranites (Comas, Zahn, Klaus, et al., 1996). All these rocks are characterized by low-P and high-T metamorphic overprint (Platt et al., 1996). Similar high-grade rocks have been previously recovered by the Deep Sea Drilling Project (DSDP) Site 121 (Hsü and Ryan, 1973), and outcrop extensively close to the border of the Alboran Sea (Fig. 1) in southern Spain (Betic Cordilleras; Vissers et al., 1995) and in northern Africa (Internal Rif; Reuber et al., 1982). They are widespread in the Alpujárride complex, which represents the intermediate tectonic unit of the Betic nappe pile (Tubía et al., 1992).

The highest temperature rocks of the Alpujárrides are located at the top of the large Sierra Bermeja and Ronda peridotite bodies (Fig. 1). In this area, granulite-facies gneisses and the peridotite are deformed along an high-T extensional shear zone (Balanyá et al., 1997). The peak T conditions recorded by these rocks are about 750°–800°C at a P of 8–13 kbar (Torres-Roldàn, 1981; Monié et al., 1994). A similar setting may be seen in the Internal Rif (Fig. 1), where cordierite (Crd) -bearing migmatites are in contact with the Beni-Bousera peridotite body (Reuber et al., 1982).

Typically the mineral assemblage of the Alpujárride basement rocks records a polyphase metamorphic evolution related to a clockwise PT path (Torres-Roldàn, 1981; Vissers et al., 1995; García-Casco and Torres-Roldàn, 1996). The presence of reaction textures and of three Al_2SiO_5 polymorphs indicates that the Alpujárride rocks underwent nearly isothermal decompression after the P peak (Loomis, 1976; Westerhof, 1977; Torres-Roldàn, 1981; García-Casco and Torres-Roldàn, 1996). The P drop has been estimated to more than 10 kbar in the high-grade rocks, as indicated by the presence of eclogite relics (Tubía and Gil-Ibarguchi, 1991). Carpholite pseudomorphs found in some Alpujárride phillites are indicative of initial P exceeding 7 kbar, even in low-grade rocks (Goffé et al., 1989).

Decompression occurred during the D_2 deformation phase (Monié et al., 1994), which produced the main foliation S_2 characterized by intergrowths of fibrolitic Sil and biotite (Bt). This tectonometamorphic event has been related to thrusting and emplacement of the Ronda peridotite body (Tubía et al., 1992), or to crustal thinning induced by extensional collapse of an overthickened crust (Platt and Vissers, 1989; Vissers et al., 1995).

The Alpujárride basement underwent nearly isobaric cooling after the isothermal decompression. The timing of the cooling is constrained by $^{40}Ar/^{39}Ar$, Rb/Sr and K/Ar ages on micas, whole rock, and amphibole. These ages show that cooling from 600° to 300°C took place at about 19 ± 1 Ma at a very high rate (Zeck et al., 1992; Monié et al., 1994). In the same time interval (20 ± 1 Ma), leucogranites generated by anatexis of crustal rocks following the emplacement of the Ronda peridotite were emplaced in the Alpujárride basement rocks (Zeck et al., 1989). Therefore the high-grade metamorphism and the subsequent cooling occurred during the late Oligocene(?)–early Miocene.

The transition from the Betic cordillera to the Alboran sea is characterized by a sudden decrease of the crustal thickness, from 35 to 15 Km (Tornè and Banda, 1992). Crustal thinning and related tectonic subsidence in the Alboran sea started during the early Miocene (Watts et al., 1993; Docherty and Banda, 1995), as deduced from commercial wells drilled close to the southern Spanish coast. Extensional tectonics is well documented in the Alboran sea and in the

[1]Zahn, R., Comas, M.C., and Klaus, A. (Eds.), 1999. *Proc. ODP, Sci. Results*, 161: College Station, TX (Ocean Drilling Program).

[2]Centro di Geodinamica, Università della Basilicata, Potenza, Italy. prosser@UNIBAS.it

[3]Dept. GEOTER, University of Udine, Via Cotonificio 114, I-33100 Udine, Italy. (Present address: Dipartimento di Scienze della Terra, Università La Sapienza, Roma, Italy.)

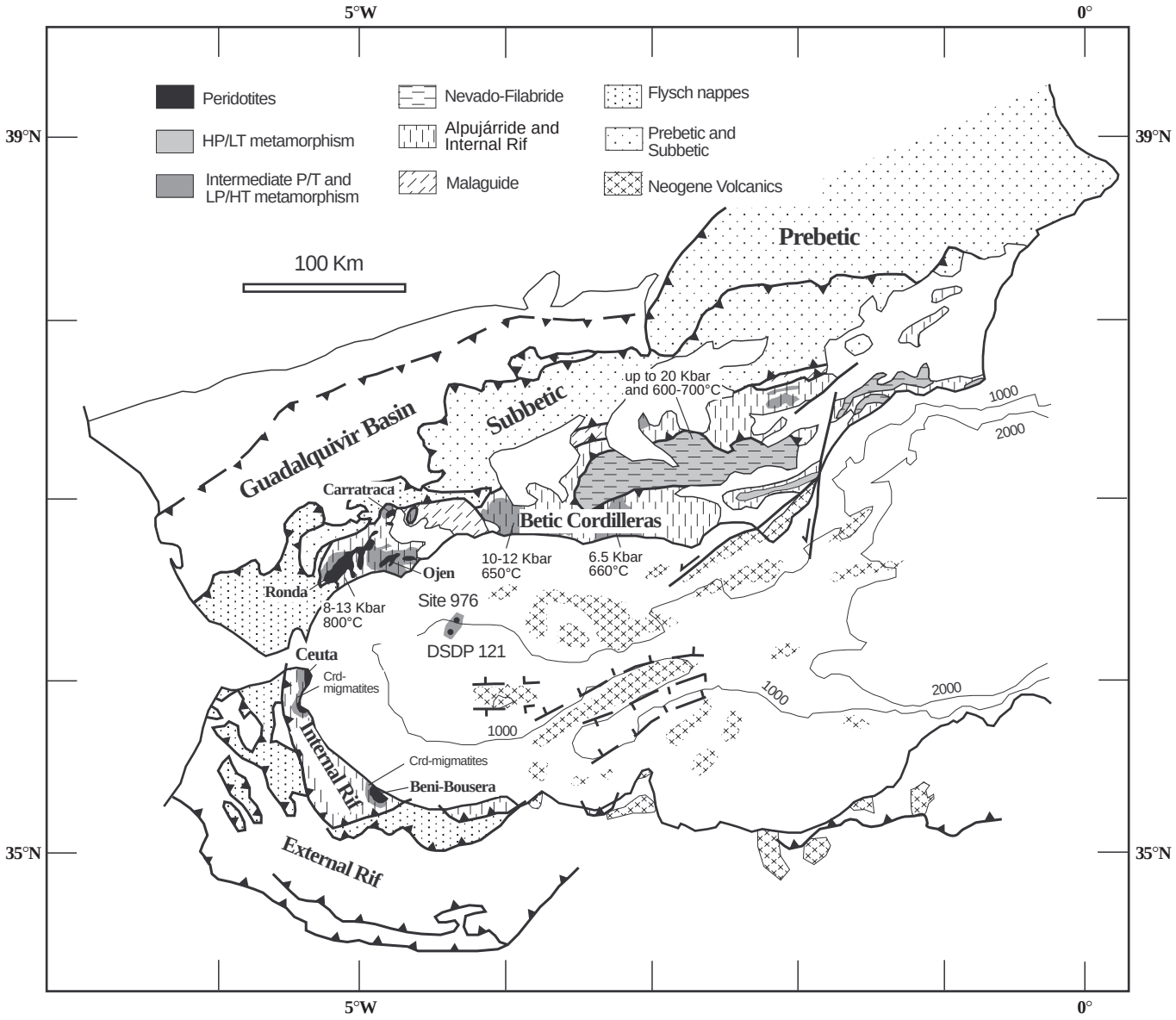

Figure 1. Sketch map of the Alboran region. Peak PT estimates for the medium to high-grade metamorphism of the Alpujárride complex after Monié et al., (1994), García-Casco and Torres-Roldán (1996), and Tubía et al. (1992). Crd-bearing migmatites in the Internal Rif chain after Reuber et al. (1982). PT estimates in the Nevado-Filabride complex after Puga et al. (1996).

southern Betic chain, which underwent NNW-SSE directed extension, followed by orogen-parallel stretching (Martínez-Martínez and Azañon, 1997). During and after the main Miocene extensional event, calk-alkaline and anatatectic magmatism took place in southern Spain, northern Africa and the Alboran sea (Hernandez et al., 1987).

In this paper we will discuss the structural and PT evolution of the Alboran basement rocks, using microstructural relationships and mineral data. To this end we will focus on the metamorphic evolution and the deformation phases recorded by schists and high-grade gneisses. In particular, we will discuss in more detail the metamorphic evolution during the main D_2 foliation-forming phase, because this stage is critical in the interpretation of the geodynamic evolution of the Alboran domain. The PT evolution is constrained by Fe-Mg^{-1} exchange thermometry (Ferry and Spear, 1978; Perchuck and Lavrent'eva, 1983) and garnet-aluminosilicate-quartz-plagioclase (GASP) barometry (Newton and Haselton, 1981). Other thermobarometric methods (e.g., Holland and Powell's database) will be applied for comparison.

HIGH-GRADE SCHISTS

The most common rock types of the Alboran basement are schists characterized with Grt-Sil-Bt-K-feldspar (Kfs)-plagioclase (Pl)-quartz (Qtz) peak mineral assemblage (Table 1). These rocks sometimes contain relics of staurolite (St) and late-stage andalusite (And) porphyroblasts. In the same sample sillimanite can be either prismatic or fibrolitic, the latter occurring along the main foliation. Muscovite (Ms) sometimes is present as inclusion in garnet, but more frequently occurs as a retrograde mineral replacing andalusite.

The protolith of the high-grade schists is a shale (Spadea and Prosser, Chap. 28, this volume) whose composition is slightly Ca- and Al-richer than the post-archean average shale (PAAS) of Taylor

Table 1. Mineral assemblages of selected samples from the Alboran Sea. Mineral abbreviations after Kretz (1983).

High-grade schists				
Sample	M_1	M_2	M_3	Notes
161-976B-				
21R-3 (Piece 1A, 33-38 cm)	Bt + St + Pl + Sil (prismatic) + Qtz	Sil (fibrolitic and prismatic) + Pl + Ksp + Qtz	And + Bt + Ksp + Pl + Qtz	Close to a calc-silicate band
82R-3 (Piece 1A, 10-13 cm)	Grt + Bt + Pl + Qtz	Bt + Pl + Ksp + Sil (fibrolitic and prismatic) + Qtz	Bt + And + Ksp + Pl + Qtz	Retrograde Ms after And
84R-1 (Piece 8B, 60-63 cm)	St + Bt + Pl + Qtz	Grt + Sil (fibrolitic and prismatic) + Bt + Pl + Ksp + Qtz	Grt + Bt + And + Ksp + Pl + Qtz + Hc	And porphyroblasts includes Hc + relict St
161-976E-				
14R-1 (Piece 3B, 40-45 cm)	Grt + St + Bt + Pl + Sil (prismatic) + Qtz	Grt + Bt + Ksp + Pl + Sil (fibrolitic and prismatic) + Qtz		
14R-3 (Piece 1A, 10-14 cm)	Grt + St + Bt + Ms + Pl + Qtz	Grt + Bt + Sil (fibrolitic) + Ksp + Qtz	Grt + Bt + And + Ksp + Qtz	Grt pseudomorphs, replaced by Bt + Qtz + Ksp; atoll-like garnets
15R-2 (Piece 3, 25-29 cm)		Crn + Hc + Bt + Ksp + Pl + Qtz		Close to a calc-silicate band; Hc includes Rt; Retrograde Ms

High-grade gneisses and migmatites				
Sample	M_2	Leucosome	M_3	Notes
161-976B-				
95R-2 (Piece 3B, 59-63 cm)	Bt + Sill + Ksp + Pl + Qtz	Ksp + Crd + Bt + Pl + Qtz	And + Crd + Ksp + Qtz (+ D_3 Sil + Bt -bearing shear zones)	Retrograde Ms
95R-3 (Piece 7, 55-59 cm)	Bt + Crn + Pl + Ksp + Qtz	Crd + Bt + Ksp + Pl + Qtz		Crn overgrows the main schistosity
97R-2 (Piece 18, 111-114 cm)	Bt + Sill + Ksp + Pl + Qtz		Grt + Crd + And + Bt + Ksp +Pl + Qtz	Rt in association with Sil and included in And
101R-2 (Piece 1, 3-6 cm)	Bt + Sil + Ksp + Pl + Qtz		And + Crd + Ksp + Qtz (+ D_3 Sil + Bt -bearing shear zones)	And overgrowing D_3 shear zones

and McLellan (1985). The Fe enrichment (FeO vs. FeO+MgO ranging between 0.71 to 0.81) and abundant graphite are features comparable with the middle to lower Paleozoic metapelites of the Alpujárride complex (Torres-Roldán, 1981).

The first mineral assemblage (M_1), consisting of Grt-Bt-staurolite (St)-Pl-Sil-Qtz ± Ms (Table 1), statically overgrows a first foliation (S_1), recorded by graphite, ilmenite, and titaniferous magnetite inclusions within staurolite, plagioclase, garnet, and by alternating Bt-rich and Pl-Qtz-rich bands (Fig. 2). In some cases it may be seen that the S_1 foliation developed parallel to the axial plane of D_1 isoclinal folds and crenulations, preserved within minerals of the M_1 assemblage (Fig. 3A). Therefore, a previous foliation (S_x) preceded the S_1 schistosity.

The second D_2 deformation event developed the main schistosity (S_2) in the axial plane of tight to isoclinal folds, which refold the D_1 crenulations preserved within Pl, St, and Grt porphyroblasts and the S_1 foliation. The S_2 foliation is characterized by folia composed of fibrolitic sillimanite and biotite intergrowths (M-domains; Bell, 1981; Vernon, 1987) intercalated between layers rich in quartz and feldspar (Q-domains). In areas where the S banding is preserved, the S_2 is still recognizable because of the preferred orientation of biotite and plagioclase crystals.

The mineral assemblage (M_2) synkinematic with the D_2 deformation is composed of the Grt-Bt-Pl-Kfs-Sil-Qtz assemblage (Table 1). Millipede structures, displaying types 2 and 3 opposedly concave microfolds (Johnson and Bell, 1996), demonstrate the synkinematic growth of garnet inner rims (Fig. 3B).

In schists from Hole 976E, characterized by centimeter-thick calc-silicate intercalations (Table 1), the M_2 mineral assemblage consists of the association Bt-Pl-Kfs-Qtz-hercynite (Hc) ± corundum (Crn). Textural evidence suggests that Crn belongs to the M_2 assemblage, because it shows synkinematic relationships with the D_2 deformation. Optically determined rutile inclusions can be observed in some Crn crystals. Sometimes schists with calc-silicate intercalations show indications for incipient partial melting, because aggregates of inclusion-free Qtz, Pl, and Kfs around Hc (Fig. 3C) can derive from the crystallization of melt pockets.

After the M_2 metamorphism, the S_2 foliation has been statically overgrown by andalusite and abundant K-feldspar porphyroblasts, belonging to the third (M_3) mineral assemblage (Table 1). In Qtz-poor and Al-rich lithologies, Hc is present in And cores, together with St relics. We interpret this texture to be indicative of the final breakdown of St, to give Hc and And.

Sometimes, late fibrolitic sillimanite can overgrow the andalusite porphyroblasts. This can imply that the M_3 crystallization occurred close to the sillimanite/andalusite phase boundary. Alternatively, a slight variation of the PT conditions occurred during or after the M_3 metamorphism. The late retrograde evolution is characterized by the replacement of andalusite and corundum crystals by abundant retrograde muscovite.

HIGH-GRADE GNEISSES AND MIGMATITIC GNEISSES

High-grade gneisses and migmatites have been recovered below the high-grade schists in Hole 976B (Fig. 1), associated with leucogranite sheets (Comas, Zahn, Klaus, et al., 1996). They are characterized by the Crd-Kfs-Sil-And-Bt-Qtz-Plg mineral association, with fibrolitic Sil occurring before or after And along the main foliation or in isolated shear zones. The gneisses range from pelitic to graywacke composition, with an Al content comparable to or lower than the PAAS (Spadea and Prosser, Chap. 28, this volume).

The contact between high-grade schists and high-grade gneisses is tectonic, because they are separated by a carbonate-cemented fault breccia. As previously stated in Comas, Zahn, Klaus, et al. (1996), the correlation of the mineral assemblages and the foliation-forming events between these two rock units is not straightforward. The gneisses lack inclusion trails related to the D_1 deformation, and a mineral assemblage comparable with the M_1 of the schists. We tried to correlate the main foliation observed in the gneisses with the S_2 of the schists, because both pre-date the growth of And porphyroblasts.

The first metamorphic assemblage of the high-grade gneisses, composed of Bt-Sil-Pl-Kfs-Qtz (Table 1), is likely correlated with the M_2 assemblage of the schists, because it is synkinematic with the S_2 foliation. Sometimes, optically determined ilmenite (Ilm) and rutile (Rt) crystals occur in association with fibrolitic sillimanite, or overgrown by later-stage Grt or And.

The S_2 foliation has been later cut by Kfs-Pl-Qtz-Crd-Bt ± Ms ± And leucosomes, related to partial melting of crustal rocks (Table 1).

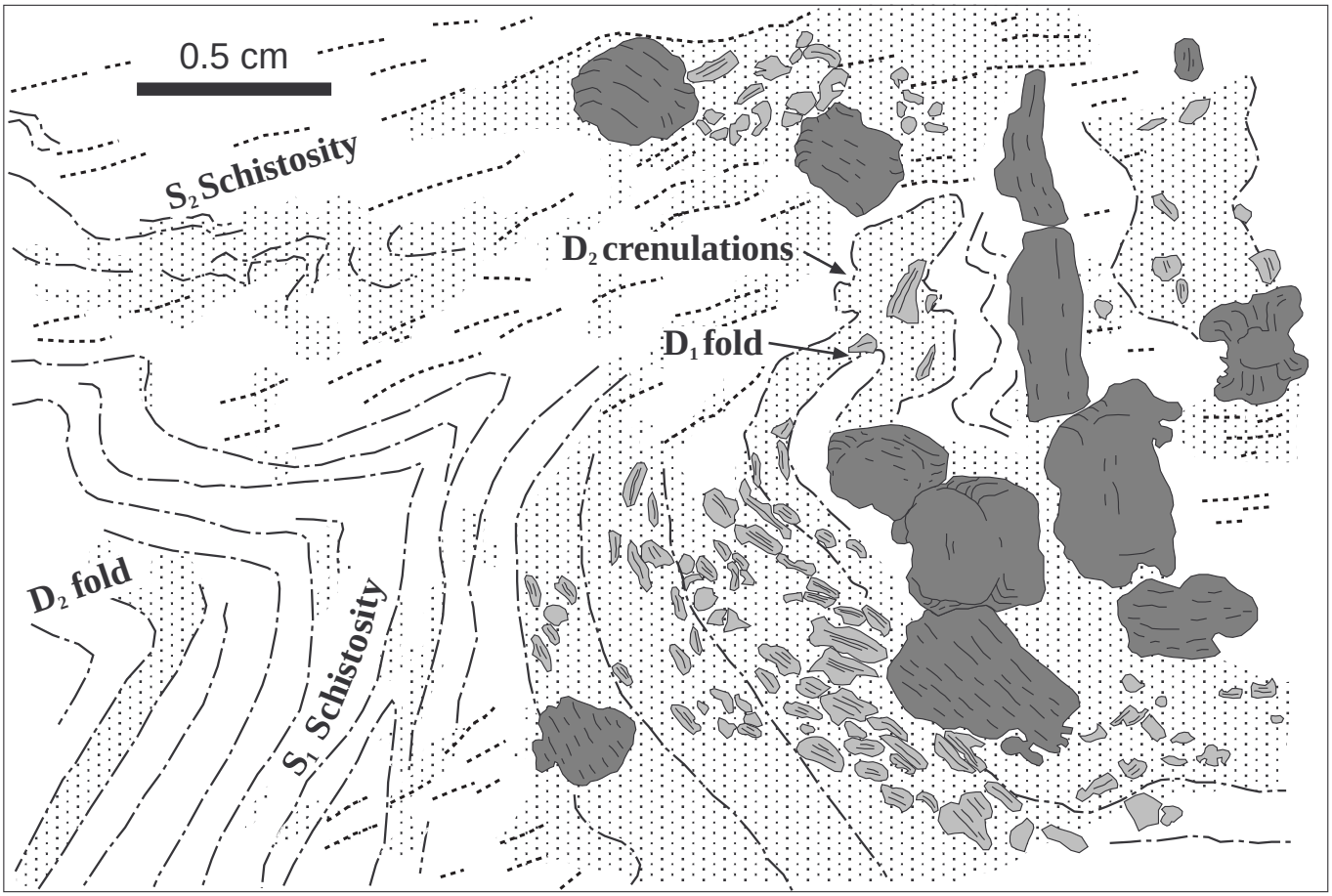

Figure 2. Relationship between D_1 and D_2 in a high-grade schist (interval 161-976E-14R-1 [Piece 3B, 40–45 cm]). Light gray = plagioclase and staurolite porphyroblasts; dark gray = garnet crystals. The stippled areas represent Bt-rich zones, generally parallel to the S_1 foliation, which is shown by dot-and-dashed lines. Dark dotted lines show the S_2 schistosity, defined by Bt and Sil. Thin lines in porphyroblasts are inclusion trails composed of graphite and titaniferous magnetite, defining the S_1 foliation. Garnet crystals show different growth stages and millipede structures.

The composition of the leucosomes, characterized by an A/CNK value of 2.2 (interval 161-976B-98R-2, 48–50 cm; Spadea and Prosser, Chap. 28, this volume), indicates that Crd probably represents restitic material, because A/CNK should not exceed 1.4-1.5 in peraluminous granites (Clarke, 1992). Sometimes, crystallization of corundum and tourmaline took place in the gneisses, close to the contact with leucosome pockets.

Further evolution of the gneisses and migmatites occurred during decreasing pressure, as indicated by the growth of andalusite, K-feldspar, cordierite-andalusite intergrowths, and garnet. This assemblage grew after the D_2 phase, because garnet and cordierite statically overgrow the S_2 Sil-bearing foliation. Therefore, it can be correlated with the M_3 assemblage found in the high-grade schists.

The M_3 metamorphism was followed by the development of Sil-bearing shear zones (S_3), which wrap around andalusite and cordierite porphyroblasts and overprint the leucosomes (Fig. 3D). Ksp crystals from the leucosome are partially replaced by myrmekite when they are in contact with the S_3 shear zones. For this reason the development of myrmekites is probably strain-induced (Simpson and Wintsch, 1989).

The crystallization relationship between sillimanite of the S_3 shear zones and andalusite can be conflicting. Typically, andalusite porphyroblasts mimetically overgrow the S_2 foliation, which is later crosscut by S_3 Sil-bearing shear zones. On the other hand, andalusite crystals can form after microfolds related to the S_3 shear zones (Fig. 3E). Therefore, the development of the S_3 probably happened close to the sillimanite/andalusite phase boundary. The final retrograde evolution is similar to the high-grade schists, with abundant muscovite growth at the expense of andalusite, sillimanite, and cordierite.

MICROSTRUCTURES AND MINERAL CHEMISTRY

Garnet of the high-grade schists occurs as 1-to 5-mm-large porphyroblasts of nearly round shape or as elongate crystals parallel to the S_1. Minerals included in garnet are mainly graphite, ilmenite and titaniferous magnetite, and, to a minor extent, biotite, staurolite, sillimanite, plagioclase, and quartz.

The rounded garnets generally display cores with scarce and coarse inclusions, inclusion-rich rims, and inclusion-poor outer rims (Fig. 4A). Inclusion trails in garnet cores can be sometimes interpreted as accumulations of displaced material along crystal facies during the first garnet growth stages. Therefore, their orientation was controlled by the orientation of the garnet crystal facies. However, rare inclusions parallel to S_1 are still recognizable in garnet cores (Figs. 2, 4A). Consequently, we can state that garnets started growing during or after the D_1 foliation-forming event.

The subsequent crystallization of the inclusion-rich garnet inner rims took place before and during the D_2 deformation. In fact, the inclusion trails bend toward parallelism with S_2 in the external part of

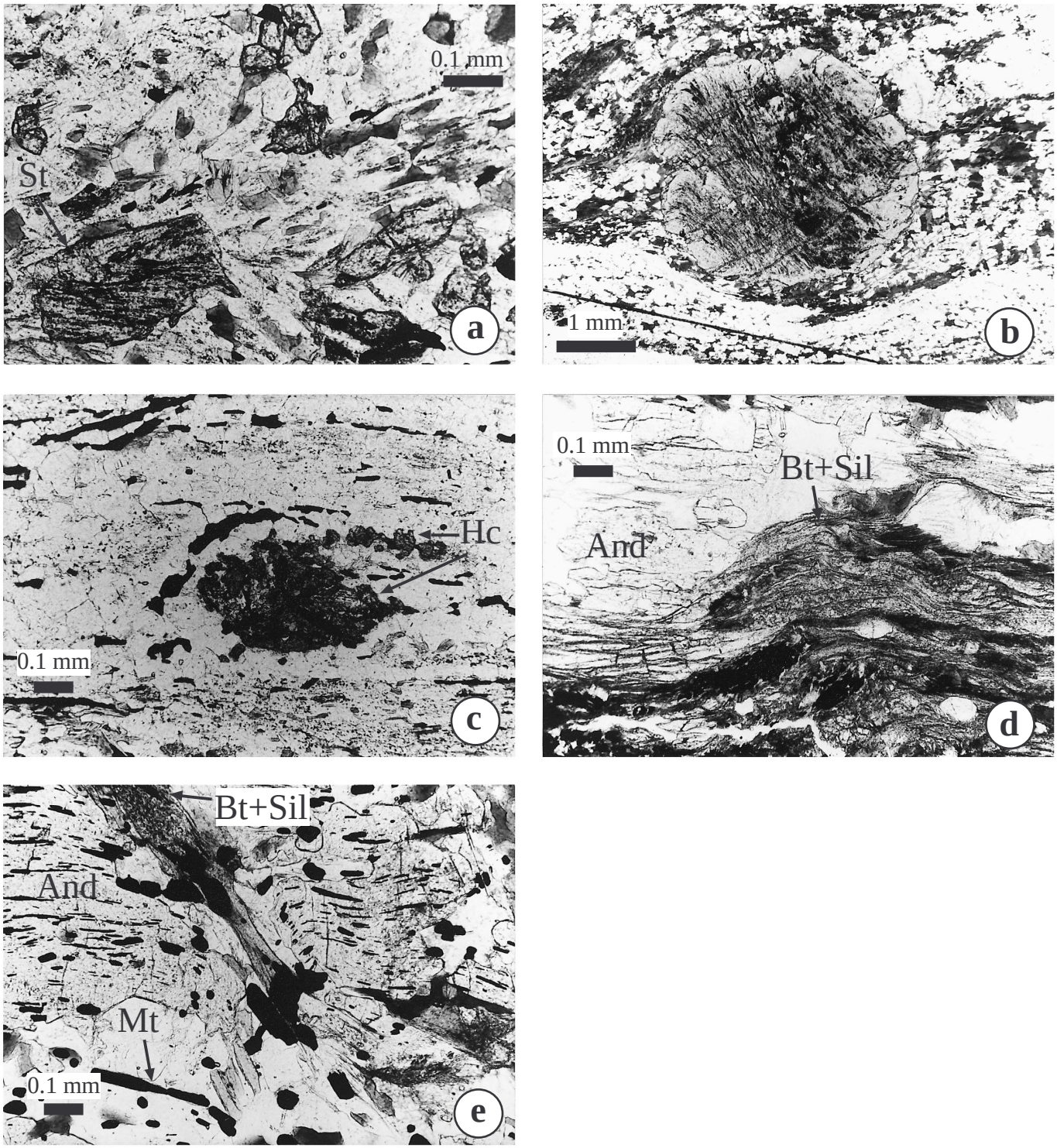

Figure 3. Textural features of high-grade schists and gneisses. **A.** D_1 isoclinal fold preserved as graphite inclusion trails within a staurolite porphyroblast. Plane-polarized light (interval 161-976B-21R-3 [Piece 1A, 33–38 cm]). **B.** Inclusion trails in garnet rim define type 2 opposedly concave microfolds (millipede structure). Matrix shows the S_2 foliation. Plane-polarized light (interval 161-976E-14R-1 [Piece 3B, 40–45 cm]). **C.** Hercynite crystals surrounded by regions consisting of inclusion-free quartz, plagioclase and K-feldspar. **D.** D_3 shear zone bordered by And porphyroblasts. Small And porphyroclasts occur within the shear zone. Crossed polars (interval 161-976B-95R-2 [Piece 1C, 22–25 cm]). **E.** Andalusite crystal overgrowing a microfold related to a S_3 shear zone. Plane-polarized light; base of photograph 1.26 mm (interval 161-976B-101R-2 [Piece 1, 3–6 cm]).

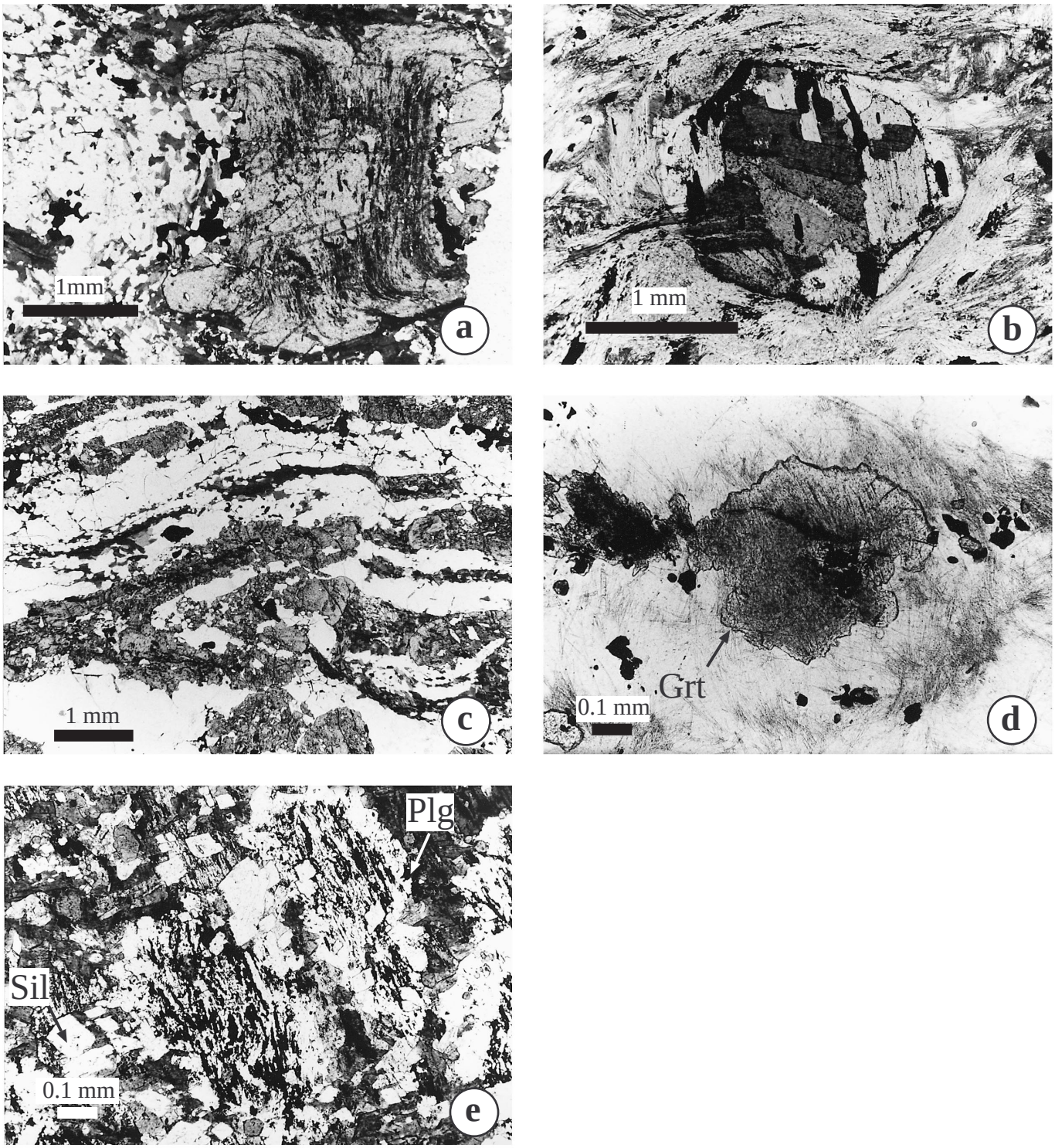

Figure 4. Mineral microstructures. **A.** Garnet displaying different growth stages. Plane-polarized light (interval 161-976E-14R-1 [Piece 3B, 40–45 cm]). **B.** Garnet partially replaced by biotite, giving an atoll-like microstructure. Plane-polarized light (interval 161-976E-14R-3 [Piece 1A, 10–14 cm]). **C.** Garnet growing mimetically on a D_1 fold. Plane-polarized light (interval 161-976E-14R-3 [Piece 1A, 10–14 cm]). **D.** Garnet overgrowing sillimanite in a high-grade gneiss. Plane-polarized light (interval 161-976B-97R-2 [Piece 18, 114–115 cm]). **E.** Plagioclases with inclusion-rich core and inclusion-poor rim. Prismatic sillimanite is enclosed within plagioclase and staurolite. Plane-polarized light (interval 161-976E-14R-1 [Piece 3B, 40–45 cm]).

the garnet inner rims (Fig. 4A). Finally, the last stage of garnet growth is represented by an inclusion-poor outer rim, from 0.1 to 0.5 mm thick (Fig. 4A). Sometimes, biotite partially replaces the inclusion-rich garnets as atoll-like structures, especially in And-bearing schists (Fig. 4B). In the Torrox nappe of the Alpujárride complex, this has been interpreted as forming during decompression (García-Casco and Torres-Roldán, 1996).

The elongate garnets are generally inclusion-rich, but they can have inclusion-poor cores. The shape of these suggests that they grew mimetically on the S_1 foliation or, sometimes, on D_1 isoclinal folds (Fig. 4C).

Garnet compositional profiles across round porphyroblasts shows bell-shaped trends for grossular (Grs) and spessartine (Sps) and concave-upward trends for almandine (Alm) and pyrope (Pyr; Fig. 5). The flat, symmetrical edges of the profile in Figure 5C can indicate garnet was re-equilibrating through diffusion. However, garnet grains with strongly different diameters (from 2.5 to 0.3 mm) show similar Alm and Pyr compositional patterns (Fig. 5C, D). Therefore, we infer that growth zoning prevails over diffusional zoning, because compositional patterns are slightly correlated to grain size. The observed decrease in the Fe/(Fe+Mg) ratio toward garnet rims (Fig. 5) indicates that garnet grew under increasing T conditions.

The compositional profiles can be slightly irregular and asymmetrical, as may be observed for the Grs trend (Fig. 5A). This latter feature can be related to some garnet dissolution, which is particularly evident along the contact between two different garnet grains. Irregularities in Grt compositional profiles can be explained by diffusional equilibration close to St or Bt inclusions (Fig. 5B).

Summing up, garnets from high-grade schists display a continuous and progressive growth, before and during the D_2 deformation. Garnet compositions can be separated into three slightly overlapping groups (Fig. 6). Cores are characterized by a wide variation in the Grs content, ranging from 20% to 10%, together with high Sps content (up to 14%). The inclusion-poor outer rims have very high Alm (about 85%) and relatively high Pyr (up to 8%) content, together with low Grs and Sps (less than 5%) content (Fig. 6).

Garnet is rarely developed in high-grade gneisses, in association with Crd. It shows moderate textural zoning and mimetically overgrows the S_2 Sil-bearing schistosity (Fig. 4D). This evidence indicates that garnet growth postdates the D_2 deformation. Garnet from

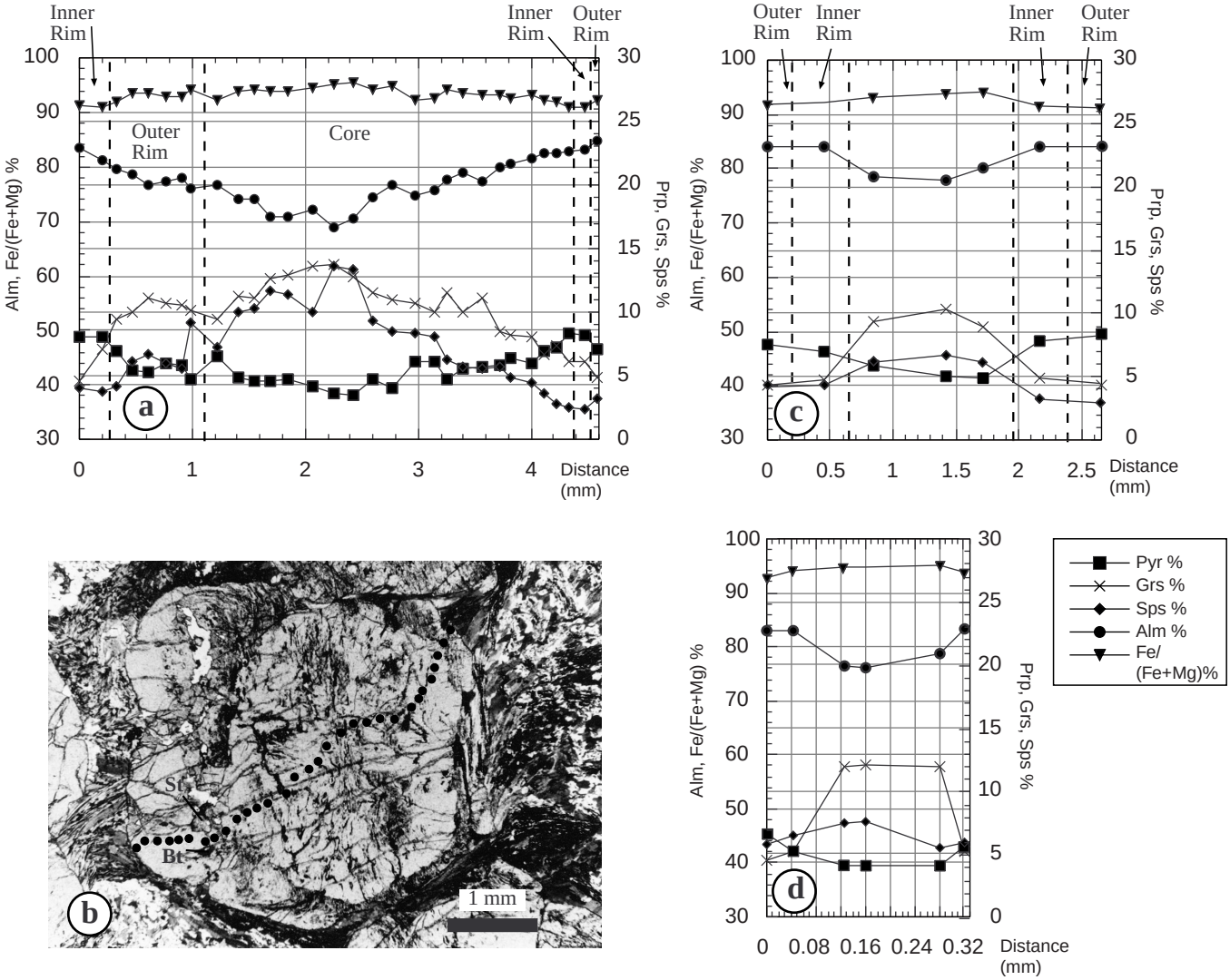

Figure 5. Compositional profiles across garnet from high-grade schists. **A.** Garnet from interval 161-976E-14R-1 [Piece 3B, 40–45 cm]. **B.** Micrograph showing the location of the compositional profile of diagram (A). Plane-polarized light. Staurolite (St) and biotite (Bt) inclusions in garnet are shown. **C.** Garnet from interval 161-976E-14R-1, 40–45 cm. **D.** Garnet from interval 161-976E-14R-3, 10–14 cm. In this diagram the horizontal scale has been expanded four times with respect to diagrams (A) and (C).

high-grade gneisses has a nearly uniform composition from core to rim (Table 2). It shows low Grs% and Sps% content, together with relatively high Alm% and Pyr%.

Plagioclase from high-grade schists have inclusion-rich cores and inclusion-free rims (Fig. 4E). Locally, inclusion trails in plagioclase cores and garnet internal rim are parallel (Fig. 2). This observation suggests that plagioclase and garnet synchronously overgrew the S_1 before the onset of the D_2 deformation. The association inclusion-rich plagioclase and staurolite (Fig. 4D), characterized by the same orientation of inclusion trails, suggests that these two phases were in equilibrium with garnet during the first M_1 metamorphism. The anorthite (An) content of plagioclase decreases toward the rim (normally from $An^{46–63}$ to $An^{42–51}$). Sometimes, even higher An values (up to An^{80}) is found in inclusion-rich plagioclase cores. Rare plagioclase inclusions within garnet display a wide variation in the An content (from An^{63} to $An^{34–35}$). The more calcic plagioclase is generally found in garnet core.

Biotite from the high-grade schists is characterized by high Al_2O_3, TiO_2, and FeO contents (Table 2), with an average Fe/(Fe+Mg) of 0.76. It occurs in the matrix, together with fibrolitic sillimanite, and as inclusions in garnet. This latter can be in contact with prismatic sillimanite or staurolite. Therefore, we suggest that the inclusion-rich garnet rim overgrew the enclosed biotite, sillimanite, and staurolite, belonging to the M_1 mineral assemblage (Fig. 7).

Matrix biotite, defining the S_2 foliation, grew in equilibrium with garnet synkinematic with the D_2 deformation. Therefore, the M_2 assemblage includes matrix biotite + sillimanite + garnet (Fig. 7). In more detail, we should consider that matrix biotite was in equilibrium with garnet areas characterized by opposedly concave microfolds and, possibly, the inclusion-poor garnet outer rim. Generally, biotite enclosed in garnet shows a slightly lower FeO content with respect to matrix biotite (Fe/[Fe+Mg] of 0.70; Table 2). This feature, together with Fe enrichment toward garnet rims, can indicate decompression, as both biotite and garnet tend to become Fe-richer while pressure decreases (Spear, 1993; García-Casco and Torres-Roldán, 1996). In gneisses and migmatites, biotite, in equilibrium with cordierite and sillimanite or andalusite (Fig. 7), has a Fe/[Fe+Mg] content of 0.63.

Cordierite from leucosomes is compositionally zoned from core to rim, with a Fe/[Fe+Mg] ratio varying between 0.25 and 0.31 (Table 2). In contrast, Crd in equilibrium with Grt has a distinctly higher Fe/[Fe+Mg] value of 0.61 (Table 2).

THERMOBAROMETRIC ESTIMATES

The PT conditions of the high-grade schists during the M_1 and M_2 metamorphic events have been compared using plagioclase, biotite, and muscovite inclusions, zoned plagioclase, and matrix biotite (Fig. 8). Thermobarometric estimates have been performed using the Grt-Bt thermometer of Perchuck and Lavrent'eva (1983), the GASP barometer of Newton and Haselton (1981), and the Grt-Pl-Ms-Qtz (Hodges and Crowley, 1985) and Grt-Pl-Bt-Qtz (Hoisch, 1990) equilibria. The calibration by Perchuck and Lavrent'eva (1983) was preferred, because the $(Al^{VI}+Ti)/(Al^{VI}+Ti+Fe+Mg)$ ratio of the biotite, ranging between 0.21 and 0.29, is higher than the value required for the application of the widely used Ferry and Spear (1978) calibration.

We obtained two different estimates using the M_1 mineral assemblage. The first one was attained using garnet core compositions (Fig. 5) and mineral inclusions. In this case the estimated PT conditions are 550°C and 5.8 kbar, within the kyanite stability field (Fig. 8A). Using garnet core and matrix plagioclase core compositions estimated P are slightly lower (5.2–5.6 kbar), but still within the kyanite stability field. This result has to be taken with some caution, because of the scarcity of data and the lack of kyanite in the Alboran basement rocks. The presence of rutile may be indicative of high pressures (Bohlen and Liotta, 1986), but this mineral is normally included in corundum and never associated with garnet in the high-grade schists.

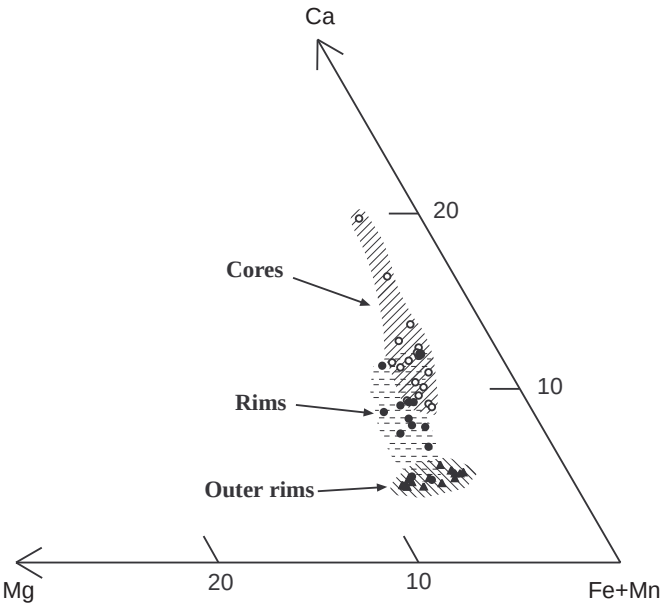

Figure 6. Garnet compositions from high-grade schists (intervals 161-976E-14R-1 [Piece 3B, 40–45 cm] and 161-976E-14R-3, 10–14 cm). Compositions can be separated into three slightly overlapping groups. Triangles = outer rim, solid circles = rim, open circles = core.

The second estimate for the M_1 mineral assemblage was derived from compositions of garnet inner rims (Fig. 5), plagioclase cores, and biotite included within garnet. We obtained a large spread for the K_{eq} lines of the Grt-Bt thermometer (Fig. 8A), probably reflecting progressive biotite re-equilibration related to prograde or retrograde metamorphism. Combining the Grt-Bt K_{eq} lines with those obtained from the GASP barometer, we can conclude that the late stage of the M_1 metamorphism took place in a T range of 570°–640°C for a P ranging between 4 and 6 kbar. These PT values are consistent with the occurrence of both staurolite and sillimanite in the M_1 mineral assemblage.

PT results obtained for M_1 were checked by using Grt inner rims, and included Bt, Pl, and Ms for one Ms-bearing sample (161-976E-14R-3 [Piece 1A, 10–14 cm]). By combining the Grt-Pl-Ms-Qtz and Grt-Pl-Bt-Qtz barometers with the Grt-Bt thermometer we obtained consistent PT values of 605°–620°C and 4.8–5.7 kbar (Fig. 8A).

The M_2 PT conditions were defined using garnet outer rim (Fig. 5) matrix biotite, and plagioclase rim compositions (Fig. 8B). Similarly to M_1, the M_2 K_{eq} lines of the Grt-Bt thermometer show a wide dispersion. However, the presence of K-feldspar and abundant sillimanite along the S_2 foliation indicates that the breakdown of muscovite has been exceeded during the growth of the M_2 mineral assemblage. Therefore, we can neglect the PT estimates falling within the Ms + Qtz field, and we can relate them to progressive re-equilibration of biotite and garnet during the retrograde evolution. Summing up, the M_2 metamorphism should have occurred at 625°–710°C and 2.8–4.4 kbar.

The PT conditions obtained from the database of Holland and Powell (1990), for $X_{H2O} = 1.0$, yield systematically higher pressures (Table 3). In addition, the calculated temperature for the M_1 mineral assemblage is higher (617° ± 26°C) than the previous estimate for the same assemblage. This latter result can indicate that biotite and plagioclase inclusions were not in equilibrium with the host garnet, or that conditions of $X_{H2O} = 1.0$ are not appropriate for the Alboran rocks. However, the occurrence of staurolite and sillimanite in the M_1 assemblage, together with the lack of kyanite, indicates that pressures calculated with the database of Holland and Powell (1990) are probably too high.

Table 2. Selected mineral analyses of high-grade schists and gneisses from Leg 161.

	High-grade schists										High-grade gneisses					Migmatites		
Core	976E-14R-1	976E-14R-1	976E-14R-1	976E-14R-1	976E-14R-1	976E-14R-3	976E-14R-1	976E-14R-1	976E-14R-1	976E-14R-3	976B-97R-2	976B-97R-2	976B-97R-2	976B-97R-2	976B-97R-2	976B-95R-2	976B-95R-2	976B-95R-2
Interval (cm)	40-45	40-45	40-45	40-45	40-45	10-14	40-45	40-45	40-45	10-14	111-114	111-114	111-114	111-114	111-114	22-25	22-25	22-25
Mineral	Grt Outer rim	Grt Rim	Grt Core	Bt Incl. in Grt	Bt Matrix	St Incl. in Grt	Pl Rim	Pl Core	Pl Incl. in Grt	Pl Incl. in Grt	Grt Int. Rim	Grt Core	Bt Matrix	Pl Matrix	Crd Close to Grt	Bt Matrix	Crd Core	Crd Rim
SiO_2	37.63	37.27	36.36	33.48	34.55	26.1	55.81	51.57	57.62	51.25	38.01	37.99	35.01	57.34	46.94	35.05	47.51	47.97
TiO_2	—	—	0.1	3.27	3.08	0.53	—	—	—	—	0.15	—	1.17	—	0.14	2.67	—	—
Al_2O_3	21.93	22.1	20.89	20.07	21.03	58.34	28.36	32.05	26.53	32.12	21.48	22.05	20.97	27.77	37	20.46	34.07	33.3
FeO	36.63	36.26	29.27	24.04	23.64	13.43	0.27	—	0.39	0.33	34.48	35.61	23.4	—	8.09	23.23	5.99	7.24
MnO	1.73	1.38	5.71	—	—	—	—	—	—	—	2.32	1.43	—	—	—	0.14	0.37	0.21
MgO	1.97	1.89	0.85	5.53	4.68	0.66	—	—	—	—	2.02	1.91	6.02	—	2.93	6.89	9.87	8.98
CaO	1.6	1.65	4.53	—	—	—	9.25	12.81	7.65	12.96	1.19	1.48	—	8.25	0.53	—	—	—
Na_2O	—	0.36	—	0.19	—	0.32	6.71	4.18	7.83	4.19	0.59	—	0.35	7.18	—	–0.77	0.78	
K_2O	—	—	—	9.21	9.22	—	—	—	0.25	—	—	—	9.05	—	1.12	9.38	—	—
Total	101.49	100.91	97.71	95.79	96.2	99.39	100.41	100.61	100.27	100.84	100.25	100.47	95.96	100.54	96.75	97.82	98.58	98.48
Oxygens	12	12	12	22	22	46	8	8	8	8	12	12	22	8	18	22	18	18
Si	2.995	2.979	3.004	5.196	5.295	7.118	2.503	2.323	2.584	2.31	3.043	3.031	5.367	2.554	4.914	5.278	4.858	4.929
Al	2.057	2.082	2.034	3.671	3.799	18.753	1.499	1.702	1.402	1.706	2.027	2.074	3.789	1.458	4.566	3.631	4.106	4.033
Fe^{3+}	—	0.016	—	0.09	0.192	—	—	—	—	—	—	—	—	—	—	0.016	—	—
Fe^{2+}	2.438	2.407	2.022	3.022	2.838	3.063	0.01	—	0.015	0.012	2.309	2.376	3.001	—	0.708	2.91	0.512	0.622
Mg	0.234	0.225	0.105	1.279	1.069	0.268	—	—	—	—	0.241	0.227	1.375	—	0.457	1.547	1.505	1.376
Ca	0.136	0.141	0.401	—	—	—	0.444	0.618	0.368	0.626	0.102	0.127	—	0.394	0.059	—	—	—
Na	—	0.056	—	0.057	—	0.169	0.583	0.365	0.681	0.366	0.091	—	0.103	0.621	—	—	0.153	0.155
K	—	—	—	1.823	1.803	—	—	—	0.014	—	—	—	1.77	—	0.15	1.802	—	—
Ti	—	—	0.006	0.382	0.355	0.109	—	—	—	—	0.009	—	0.135	–0.011	0.302	—	—	
Mn	0.117	0.093	0.4	—	—	—	—	—	—	—	0.157	0.097	—	—	—	0.018	0.032	0.018
Total Cat.	7.977	8	7.972	15.528	15.352	29.481	5.04	5.008	5.063	5.02	7.98	7.932	15.54	5.027	10.866	15.505	11.165	11.133
Fe/(Fe+Mg)	0.91	0.91	0.95	0.70	0.73	0.92	—	—	—	—	0.91	0.91	0.69	—	0.61	0.65	0.25	0.31
Alm%	83.35	83.985	69.057	—	—	—	—	—	—	—	82.2	84.047	—	—	—	—	—	—
Prp%	8	7.8507	3.5861	—	—	—	—	—	—	—	8.5796	8.0297	—	—	—	—	—	—
Grs%	4.6496	4.9197	13.695	—	—	—	—	—	—	—	3.6312	4.4924	—	—	—	—	—	—
Sps%	4	3.2449	13.661	—	—	—	—	—	—	—	5.5892	3.4312	—	—	—	—	—	—
Ab%	—	—	—	—	—	—	56.761	37.126	64.065	36.911	—		—	61.183	—	—	—	—
An%	—	—	—	—	—	—	43.239	62.874	34.589	63.089	—		—	38.817	—	—	—	—

Notes: Samples from Cores 161-976E-14R-1 and 976E-14R-3 are high-grade schists, while sample from Core 976E-95R-2 is a high-grade gneiss. Analyses were obtained by a Cambridge S360 SEM equipped with a LINK AN 1000ED detector (CNR Chimica dei Plasmi, instrument hosted in Dip. Geomineralogico, University of Bari). Operation conditions were: 15 kV accelerating potential, 1 nA probe current. For standardization several minerals and pure compounds manufactured by Micro-Analysis Consultants Ltd were used. Fe^{3+} in biotite has been calculated using the Dymek (1983) approach.

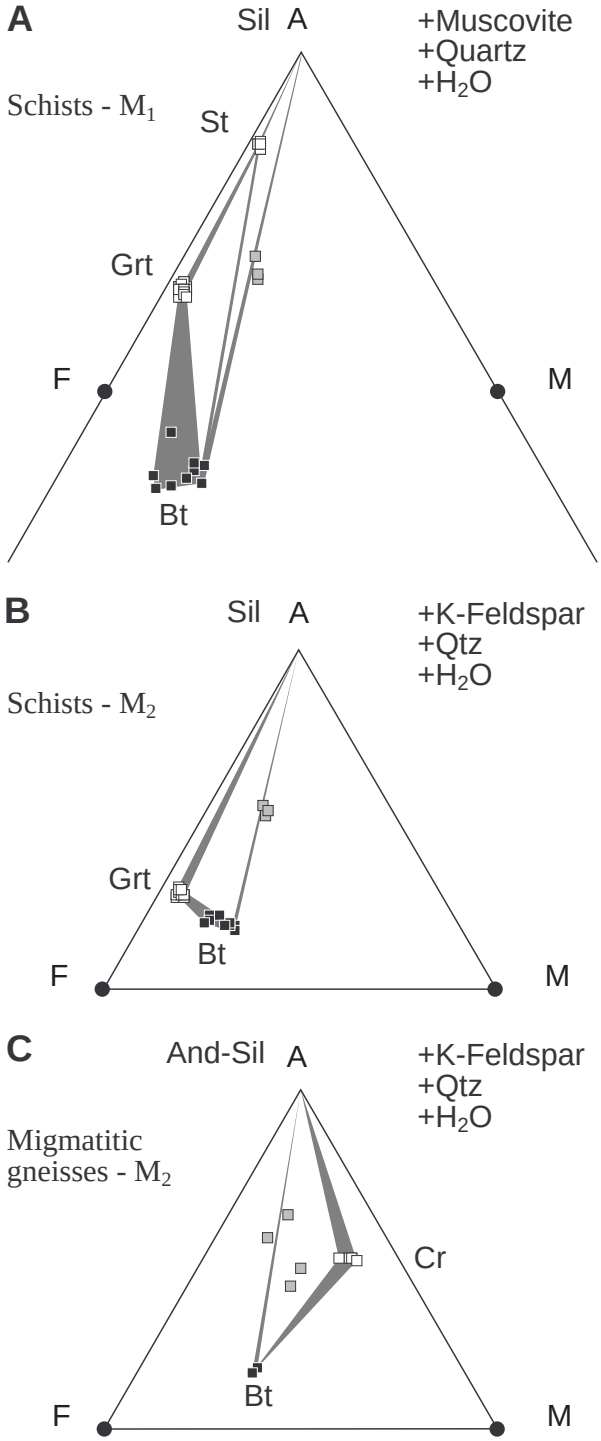

Figure 7. AFM diagrams for high-grade schists and gneisses. FeO value of biotite has been calculated using the method proposed by Dymek (1983). Open squares represents St, Grt, and Crd compositions. Black squares represent Bt compositions. **A.** M_1 mineral association (Grt-St-Sil-Bt-Ms with Bt and Ms enclosed in Grt); gray squares represent the composition of some Al-silicate (Als) Bt-bearing schists (Spadea and Prosser, Chap. 28, this volume). **B.** M_2 mineral association (Grt-Sil-Bt-Kfs with matrix Bt) plotted together with Als-Bt-bearing schists. **C.** Minerals and bulk-rock composition (gray squares) from Crd-Bt-Kfs-Sil-And-bearing migmatitic gneisses.

PT conditions of the high-grade gneisses have been estimated only for the late M_3 assemblage (Fig. 9), using Grt-Bt thermometry (Perchuck and Lavrent'eva, 1983) and the Crd-Grt-Sil-Qtz barometer (Nichols et al., 1992). We obtained a T of 595-610 Kbar, for distinctly lower P of 1.25–1.75 kbar. This result is consistent with the occurrence of the reaction Bt + Al-silicate (Als) → Grt + Crd in the high-grade gneisses.

PT EVOLUTION

All thermobarometric methods indicates that: (1) peak temperature during M_2 was about 700°C (708° ± 47°C, using the database of Holland and Powell, 1990), for P values spanning from 2.8 to 4.4 kbar; (2) the evolution from M_1 to M_2 was related to a decrease in P associated to a T increase. The peak metamorphic conditions were reached close to the Bt-dehydration melting curve during or just after the D_2 deformation (Fig. 10). Further evidence for high-T peak metamorphic conditions can be deduced on the basis of the following textural observations:

1. In banded schists, interbedded between calc-silicate layers, hercynitic spinel, associated to Fe-Ti oxides, occurs within biotite-free regions, consisting of inclusion-free plagioclase, K-feldspar, and quartz. This textural evidence suggests that biotite was consumed and hercynite, Fe-Ti oxides, and melt were produced, possibly by a Bt-dehydration melting reaction.
2. The presence of corundum bordered by K-feldspar in the high-grade schists and migmatitic gneisses is probably related to a muscovite-consuming reaction: Ms → Crn + Kfs + H_2O (Spear and Parrish, 1996), taking place at about 700°C for P conditions of 3–4 kbar (Fig. 10). This reaction occurred during the M_2, and therefore it consumed previous Ms belonging to the M_1 mineral assemblage.

The PT conditions of the high-grade gneisses during M_2 are less well constrained. Partial melting producing the Crd-bearing leucosomes likely originated from a Bt-dehydration melting reaction: Bt + Als + Qtz + Vapor → Crd + Melt (Fig. 10; Vielzeuf and Holloway, 1988), with cordierite occurring as a restitic phase. This reaction takes place at PT conditions consistent with the M_2 metamorphism (Fig. 10).

In high-grade schists the PT conditions during the M_3 are constrained by the presence of K-feldspar, close to the andalusite/sillimanite phase boundary (Fig. 10). Therefore, the M_3 metamorphism took place in the retrograde portion of the PT path, at about 625°C and 2 kbar. This estimate is in agreement with the PT conditions calculated for the high-grade gneisses using thermobarometric methods. Further retrogression led to the instability of andalusite, which was replaced by muscovite.

CONCLUSIONS

The basement recovered at Site 976 records high-T conditions (about 700°C) with a clockwise PT path (Fig. 10). The main deformation phase (D_2) occurred close to the metamorphic peak, and was associated with partial melting. Later shear zones (D_3) developed during decreasing P and T conditions.

The PT evolution of the Alboran Sea basement is quite different from most of the PT paths followed by the Alpujárride nappes of the western Betic chain (Fig. 10). In particular, the nearly isothermal decompression after the PT-peak, frequently shown by the Alpujárrides (Torres-Roldàn, 1981; Monié et al., 1994; García-Casco and Torres-

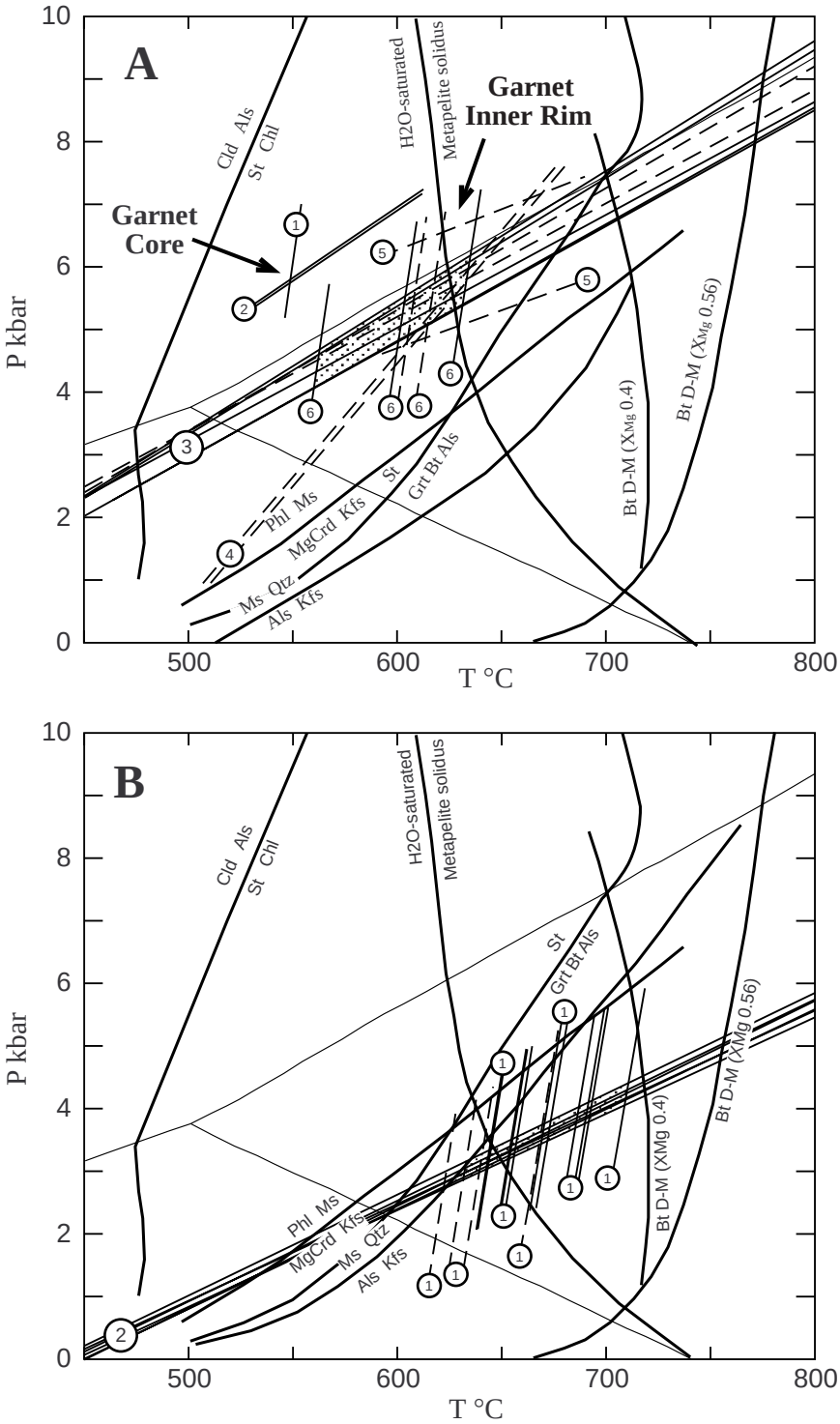

Figure 8. Thermobarometric estimates using Grt-Bt thermometry coupled with GASP, Grt-Pl-Ms-Qtz, and Grt-Pl-Bt-Qtz barometry. **A.** M_1 mineral assemblage. 1 = Grt cores and Bt included within the inner part of Grt. 2 = Grt cores and Pl included within Grt. 3 = Grt inner rims and cores of matrix Pl. 4 = Grt inner rims and included Pl and Ms. 5 = Grt inner rims and included Pl and Bt. 6 = Bt included in inner Grt rims. **B.** M_2 mineral assemblage. 1 = Grt external rims and rims of matrix Pl. 2 = Grt external rims and matrix Bt. The stippled areas represent likely metamorphic conditions for the M_1 and M_2 metamorphism in the high-grade gneisses. In both diagrams the following samples were used to obtain the K_{eq} lines: interval 161-976E-14R-1 (Piece 3B, 40–45 cm) (solid lines) and interval 161-976E-14R-3 (Piece 1A, 10–14 cm) (dashed lines). Al_2SiO_5 phase relations after Chatterjee, 1991. Cld + Als = St + Chl and St = Grt + Bt + Als (KFMASH system) after Spear (1993). Phl + Ms = MgCrd + Kfs (KMASH system) after Spear (1993). H_2O-saturated metapelite solidus after Thompson (1982). Ms + Qtz = Als + Kfs at $P_{tot} = P_{H2O}$ (Helgeson et al., 1978). Bt dehydration melting at $X_{Mg} = 0.4$ (calculated; Clemens, 1984). Bt dehydration melting at $X_{Mg} = 0.56$ (Le Breton and Thompson, 1988).

Roldán, 1996), has not been recognized in the present study. Moreover, in the basement of the Alboran Sea the peak P should have occurred before the peak T, which is an uncommon feature for the Alpujárride nappes.

However, the coincidence of the main D_2 deformation phase with the peak metamorphism and the occurrence of a D_3 phase during decreasing pressures has been recognized elsewhere in the Alpujárride units (Tubía et al., 1992). In addition, a peak T following the peak P has been described by Bakker et al. (1989) for the Alpujárride units of the eastern Betic chain (Fig. 10).

In the western Betics or the Internal Rif (Fig. 1), high P/T metamorphism related to the main nappe-forming event was followed by extension and vertical shortening (Balanyá et al., 1997). This process uplifted hot mantle material to higher crustal levels and triggered low

Table 3. PT estimates and reactions used for the thermobarometric estimates.

N	Sample	Assemblage	PT conditions
1	Interval 161-976E-	M_1	T = 617 ± 26°C
	14R-1 (Piece 3B, 40-45 cm)	Grt core + Pl inclusion + Bt inclusion + St + Als + Qtz	P = 8.0 ± 1.0 kbar
2	Interval 161-976E-	M_1	T = 650 ± 26°C
	14R-3 (Piece 1A, 10-14 cm)	Grt internal rim + Pl core + Bt inclusion + Als + Qtz	P = 6.5 ± 1.1 kbar
3	Interval 161-976E-	M_2	T = 692 ± 47°C
	14R-3 (Piece 1A, 10-14 cm)	Grt rim + Pl rim + Bt + Ksp + Als + Qtz	P = 6.5 ± 1.4 kbar
4	Interval 161-976E-	M_2	T = 708 ± 47°C
	14R-1 (Piece 3B, 40-45 cm)	Grt rim + Pl rim + Bt + Ksp + Als + Qtz	P = 5.3 ± 1.4 kbar

Equilibria used for PT determinations N.1 and 2:
23Grs + 6Mg-St + 48Qtz = 8Pyr + 69An + 12H_2O
75An + 6Mg-St = 8Pyr + 25Grs + 96Ky + 12H_2O
23Grs + 6Fe-St + 48Qtz = 8Alm + 69An + 12H_2O
Pyr + 2Grs + 3East + 6Qtz = 6An + 3Phl
2Grs + 3Alm + 3East + 6Qtz = 2Pyr + 6An + 3Ann
12An + 3Phl + 4Na-Phl = 5Pyr + 4Grs + 4Ab + 3East + 4H_2O

Equilibria used for PT determinations N.3 and 4:
Pyr + 2Grs + 3East + 6Qtz = 3Phl + 6An
4Grs + 3Phl + 12Sil = Pyr + 3East + 12An
Phl + 6An = Pyr + 2Grs + Kfs + 3Sill + H_2O (for PT determination 4)
7Phl + 12An = 5Pyr + 4Grs + 3East + 4Ksp + 4H_2O (for PT determination 3)
Na-Phl + 6An = Pyr + 2Grs + Ab + 3Sil + H_2O
Ann + 6An = 2Grs + Alm + Kfs + 3Sil + H_2O

Note: Estimates made following the data set of Holland and Powell (1990), for X_{H20} = 1.0.

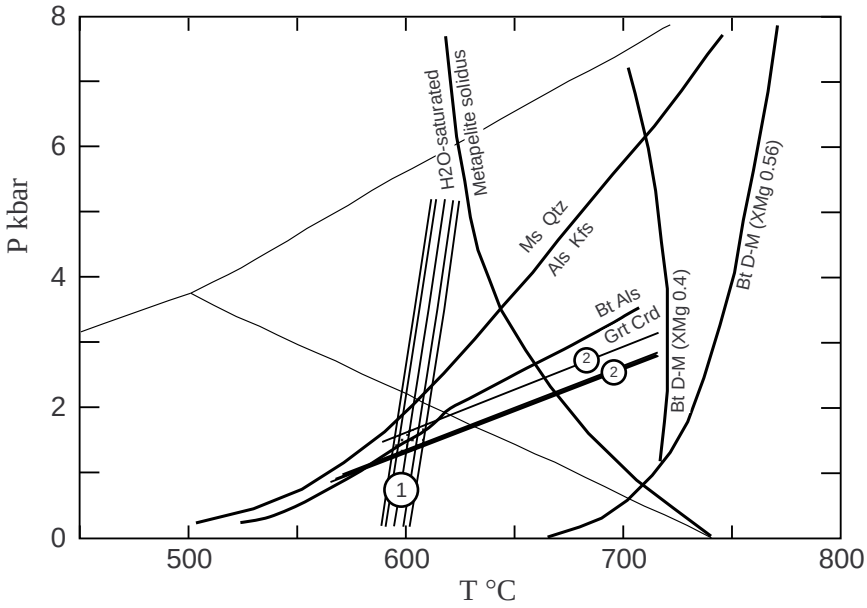

Figure 9. Thermobarometric estimates using Grt-Bt thermometry coupled with Grt–Crd–Sil–Qtz barometry in high-grade gneisses. 1 = Grt cores and inner rims and matrix Bt. 2 = Grt cores and inner rims and Crd. The stippled area represents likely metamorphic conditions for the M_3 metamorphism in the high-grade gneisses. The K_{eq} lines have been obtained using Sample 161-976B-97R-2 (Piece 18, 111–114 cm). Bt + Als = Grt + Crd (KFMASH system) after Spear (1993). The other reaction curves as in Figure 8.

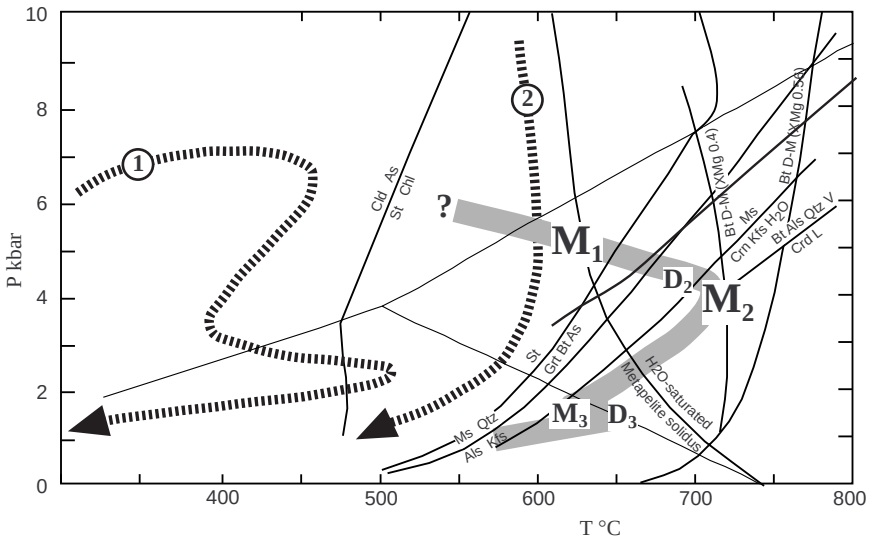

Figure 10. Inferred PT path for the Alboran high-grade schists and gneisses. The approximate location of the M_1, M_2, and M_3 metamorphic events is indicated on the PT path. 1 = PT path for the Almanzora unit (eastern Alpujárrides) after Bakker et al. (1989). 2 = PT path for graphitic schists in the Torrox unit (Western Alpujárrides), after Monié et al. (1994). Bt + Als + Qtz + Vapor = Crd + Melt after Vielzeuf and Holloway (1988); Ms = Crn + Kfs + H_2O after Spear and Parrish (1996). The other reaction curves as in Figure 8.

P/T metamorphism. In the Alboran basement crustal thinning, coupled with substantial thinning of the mantle lithosphere (Sandiford and Powell, 1986), can explain contemporaneous heating and decompression between D_1 and D_2. Moreover, magmatic underplating during extension could take into account the persistence of high-T conditions at very low P during M_3. This interpretation is consistent with the shallow moho depth reported for the Alboran sea (Torné and Banda, 1992), and with the protracted volcanic activity during Miocene (Hernandez et al., 1987).

The age of metamorphism of the Alboran basement rocks should be similar to the lower Miocene ages obtained for the Betic cordilleras (Platt et al., 1996). Fast exhumation and cooling rates after the high-grade metamorphism are indicated by the short time difference between these ages and the Serravallian age of the marine sediments that cover the Alboran basement. A further evidence of fast cooling comes from a biotite K-Ar cooling age of 16±1 Ma, obtained by Steiger and Frick (1973) from rocks of the Alboran basement at DSDP Site 121 (Fig. 1).

The presence of widespread cataclastic bands and the scarcity of low-T plastic deformation is in agreement with a short residence time of the Alboran rocks in the middle-upper crust at high-T conditions. On the contrary, they cooled down rapidly after the high-T metamorphism.

ACKNOWLEDGMENTS

This paper benefited from fruitful discussions with Alfredo Caggianelli and Erwin Gueguen. Many thanks to Pasquale Acquafredda (Dip. Geomineralogico, University of Bari) for the analytical facilities. Thermobarometric calculations were performed with the programs Thermobarometry by Kohn and Spear, and Thermocalc by Holland and Powell. Biotite formulas were calculated using the program Bt by Alfredo Caggianelli. Reviews by Virginia B. Sisson and Ronan Hebert are gratefully acknowledged.

REFERENCES

Bakker, H.E., De Jong, K., Helmers, H., and Biermann, C., 1989. The geodynamic evolution of the internal zone of the Betic Cordilleras (south-east Spain): a model based on structural analysis and geothermobarometry. *J. Metamorph. Geol.,* 7:359–381.

Balanyá, J.C., García-Dueñas, V., Azañón, J.M., 1997. Alternating contractional and extensional events in the Alpujarride nappes of the Alboran domain (Betics, Gibraltar arc). *Tectonics,* 16:226–238.

Bell, T.H., 1981. Foliation development - the contribution, geometry and significance of progressive, bulk, inhomogeneous shortening. *Tectonophysics,* 75:273–296.

Bohlen, S.R., and Liotta, J.J., 1986. A barometer for garnet amphibolites and garnet granulites. *J. Petrol.,* 27:1025–1034.

Chatterjee, N.D., 1991. *Applied Mineralogical Thermodynamics:* Berlin (Springer-Verlag).

Clarke, D.B., 1992. *Granitoid Rocks:* London (Chapman & Hall).

Clemens, J.D., 1984. Water contents of silicic to intermediate magmas. *Lithos,* 17:273–287.

Comas, M.C., Zahn, R., Klaus, A., et al., 1996. *Proc. ODP, Init. Repts.,* 161: College Station, TX (Ocean Drilling Program).

Docherty, C., and Banda, E., 1995. Evidence for the eastward migration of the Alboran Sea based on regional subsidence analysis: a case for basin formation by delamination of the subcrustal lithosphere? *Tectonics,* 14:804–818.

Dymek, F.R., 1983. Titanium, aluminum and interlayer cation substitution in biotite from high-grade gneisses, West Greenland. *Am. Mineral.,* 68:880–899.

Ferry, J.M., and Spear, F.S., 1978. Experimental calibration of the partitioning of Fe and Mg between biotite and garnet. *Contrib. Mineral. Petrol.,* 66:113–117.

García-Casco, A., and Torres-Roldán, R.L., 1996. Disequilibrium induced by fast decompression in St-Bt-Grt-Ky-Sil-And metapelites from the Betic Belt (Southern Spain). *J. Petrol.,* 37:1207–1239.

Goffé, B., Michard, A., García-Dueñas, V., González Lodeiro, F., Monié, P., Campos, J., Galindo-Zaldivar, J., Jabaloy, A., Martínez-Martínez, J.M., and Simancas, F., 1989. First evidence of high-pressure, low-temperature metamorphism in the Alpujarride nappes, Betic Cordilleras (S.E. Spain). *Eur. J. Mineral.,* 1:139–142.

Helgeson, H.C., Delany, J.M., Nesbitt, H.W., and Bird, D.K., 1978. Summary and critique of the thermodynamic properties of rock-forming minerals. *Am. J. Sci.,* 278A.

Hernandez, J., de Larouzière, F.D., Bolze, J., and Bordet, P., 1987. Le magmatisme néogène bético-rifain et le couloir de décrochement trans-Alboran. *Bull. Soc. Geol. Fr.,* 3:257–267.

Hodges, K.V., and Crowley, P.D., 1985. Error estimation and empirical geothermobarometry for pelitic systems. *Am. Mineral.,* 70:702–709.

Hoisch, T.D., 1990. Empirical calibration of six geobarometers for the mineral assemblage quartz + muscovite + biotite + plagioclase + garnet. *Contrib. Mineral. Petrol.,* 104:225–234.

Holland, T.J.B., and Powell, R., 1990. An enlarged and updated internally consistent dataset with uncertainties and correlations: the system K_2O-Na_2O-CaO-MgO-MnO-FeO-Fe_2O_3-Al_2O_3-TiO_2-SiO_2-C-H_2-O_2. *J. Metamorph. Geol.,* 8:89–124.

Hsü, K.J., and Ryan, W.B.F., 1973. Comments on Alboran basin basement samples. *In* Ryan, W.B.F., Hsü, K.J., et al., *Init. Repts. DSDP,* 13: Washington (U.S. Govt. Printing Office), 762–766.

Johnson, S.E., and Bell, T.H., 1996. How useful are "millipede" and other similar porphyroblast microstructures for determining synmetamorphic deformation histories? *J. Metamorph. Geol.,* 14:15–28.

Kretz, R., 1983. Symbols for rock-forming minerals. *Am. Mineral.,* 68:277–279.

Le Breton, N., and Thompson, A.B., 1988. Fluid-absent (dehydration) melting of biotite in metapelites in the early stages of crustal anatexis. *Contrib. Mineral. Petrol.,* 99:226–237.

Loomis, T.P., 1976. Irreversible reactions in high-grade metapelitic rocks. *J. Petrol.,* 17:559–588.

Martínez-Martínez, J.M., and Azañón, J.M., 1997. Mode of extensional tectonics in the southeastern betics (SE spain): implications for the tectonic evolution of the peri-alboran orogenic system. *Tectonics,* 16:205–225.

Monié, P., Torres-Roldán, R.L., and García-Casco, A., 1994. Cooling and exhumation of the western Betic Cordilleras, $^{40}Ar/^{39}Ar$ thermochronological constraints on a collapsed terrane. *Tectonophysics,* 238:353–379.

Newton, R.C., and Haselton, H.T., 1981. Thermodynamics of the garnet-plagioclase-Al_2SiO_5-quartz geobarometer. *In* Newton R.C. (Ed.), *Thermodynamics of Minerals and Melts:* New York (Springer-Verlag), 131–147.

Nichols, G.I., Berry, R.F., and Green, D.H., 1992. Internally consistent gahnitic spinel-cordierite-garnet equilibria in the FMASHZn system: geothermobarometry and applications. *Contrib. Mineral. Petrol.,* 111:362–377.

Passchier, C.W., Myers, J.S., and Kröner A., 1990. *Field Geology of High-Grade Gneiss Terrains:* Berlin (Springer-Verlag).

Perchuk, L.L., and Lavrent'eva, I.V., 1983. Experimental investigation of exchange equilibria in the system Cordierite-garnet-biotite. *In* Saxena, S.K. (Ed.), *Kinetics and Equilibrium in Mineral Reactions:* Berlin (Springer-Verlag), 199–239.

Platt, J.P., Soto, J.I., Comas, M.C., and Leg 161 Shipboard Scientists, 1996. Decompression and high-temperature–low-pressure metamorphism in the exhumed floor of an extensional basin, Alboran Sea, Western Mediterranean. *Geology,* 24:447–450.

Platt, J.P., and Vissers, R.L.M., 1989. Extensional collapse of thickened continental lithosphere: a working hypothesis for the Alboran Sea and Gibraltar Arc. *Geology,* 17:540–543.

Puga, E., Nieto, J.M., Diaz De Federico, A., Portugal, M., and Reyes, E., 1996. The intra-orogenic Soportújar Formation of the Mulhacén Complex: Evidence for the polyciclic character of the Alpine orogeny in the Betic Cordilleras. *Eclogae Geol. Helv.,* 89:129–162.

Reuber, I., Michard, A., Chalcouan, A., Juteau, T., and Jermoumi, B., 1982. Structure and emplacement of the Alpine type peridotites from Beni Bousera, Rif, Morocco: a polyphase tectonic interpretation. *Tectonophysics,* 82:231–251.

Sandiford, M., and Powell R., 1986. Deep-crustal metamorphism during continental extension: modern and ancient examples. *Earth Planet. Sci. Lett.,* 79:151–158.

Simpson, C., and Wintsch, R.P., 1989. Evidence for deformation-induced K-feldspar replacement by myrmekite. *J. Metamorph. Geol.,* 7:261–275.

Spear, F.S., 1993. *Metamorphic Phase Equilibria and Pressure-Temperature-Time Paths:* Washington (Mineral. Soc. Am.), Monogr. 1.

Spear, F.S., and Parrish, R.R., 1996. Petrology and cooling rates of the Valhalla Complex, British Columbia, Canada. *J. Petrol.*, 37:733–765.

Steiger, R.H., and Frick, U., 1973. Isotopic dating of Alboran "basement." *In* Ryan, W.B.F., Hsü, K.J., et al., *Init. Repts. DSDP,* 13 (Pt. 2): Washington (U.S. Govt. Printing Office), 762.

Taylor, S.R., and McLennan, S.M., 1985. *The Continental Crust: Its Composition and Evolution:* Oxford (Blackwell Scientific).

Thompson, A.B., 1982. Dehydration melting of pelitic rocks and the generation of H2O-undersaturated granitic liquids. *Am. J. Sci.*, 282:1567–1595.

Torné, M., and Banda, E., 1992. Crustal thinning from the Betic Cordillera to the Alboran Sea. *Geo-Mar. Lett.*, 12:76–81.

Torres-Roldán, R.L., 1981. Plurifacial metamorphic evolution of the Sierra Bermeja peridotite aureole (southern Spain). *Estud. Geol. (Madrid)*, 37:115–133.

Tubía, J.M., Cuevas, J., Vilà, F.N., Alvarez, F., and Aldalya, F., 1992. Tectonic evolution of the Alpujárride Complex (Betic Cordillera, southern Spain). *J. Struct. Geol.*, 14:193–203.

Tubía, J.M., and Gil-Ibarguchi, J.I., 1991. Eclogites of the Ojen nappe: a record of subduction in the Alpujárride complex (Betic Cordilleras, southern Spain). *J. Geol. Soc. London*, 148:801–804.

Vernon, R.H., 1987. Growth and concentration of fibrous sillimanite related to heterogeneous deformation in K-feldspar-sillimanite metapelites. *J. Metamorph. Geol.*, 5:51–68.

————, 1996. Problems with inferring P-T-t paths in low-P granulite facies rocks. *J. Metamorph. Geol.*, 14:143–153.

Vielzeuf, D., and Holloway, J.R., 1988. Experimental determination of the fluid-absent melting relations in the pelitic system: consequences for crustal differentiation. *Contrib. Mineral. Petrol.*, 98:257–276.

Vissers, R.L.M., Platt, J.P., and van der Wal, D., 1995. Late orogenic extension of the Betic Cordillera and the Alboran Domain: a lithospheric view. *Tectonics*, 14:786–803.

Watts, A.B., Platt, J.P., and Buhl, P., 1993. Tectonic evolution of the Alboran Sea Basin. *Basin Res.*, 5:153–177.

Westerhof, A.B., 1977. On the contact relations of high-temperature peridotites in the Serrania de Ronda, southern Spain. *Tectonophysics*, 39:579–591.

Zeck, H.P., Albat, F., Hansen, B.T., Torres-Roldán, R.L., and García-Casco, A., 1989. Alpine tourmaline-bearing muscovite leucogranites, intrusion ages and petrogenesis, Betic Cordilleras, Spain. *N. Jahrb. Miner. Monatsh.*, 11:513–520.

Zeck, H.P., Monié, P., Villa, I.M., and Hansen, B.T., 1992. Very high rates of cooling and uplift in the Alpine belt of the Betic Cordilleras, southern Spain. *Geology*, 20:79–82.

Date of initial receipt: 19 May 1997
Date of acceptance: 2 December 1997
Ms 161SR-219